J. Fluid Mech. (1985), *vol.* 152, *pp.* 479–499
Printed in Great Britain

Nonlinear progressive edge waves: their instability and evolution

By HARRY H. YEH
Department of Civil Engineering, University of Washington, Seattle, Washington 98195, U.S.A.

(Received 3 April 1984 and in revised form 27 August 1984)

The fundamental properties of nonlinear progressive edge waves are investigated experimentally in a physical model with a uniformly and mildly sloping beach with a straight shoreline. An evolution equation for the envelope of progressive edge waves is the nonlinear Schrödinger (NLS) equation. It is found that the timescale of viscous-dissipation effects in the experiments is comparable with the timescale of the theoretical evolution process for inviscid progressive edge waves. This lack of timescale separation indicates a major shortcoming of the NLS equation as a model of the laboratory experiments. Even with this limitation, a uniform train of edge waves is found to be unstable to a modulational perturbation as predicted by the NLS equation. However, behaviour of the evolution is both qualitatively and quantitatively different from the theoretical predictions. The evolution of the periodogram for the unstable wavetrain shows an asymmetric development of the sidebands about the fundamental frequency; instability growth is limited to the lower sideband. This behaviour leads to a sequential shift of wave energy to lower frequencies as the waves propagate. It is found that a locally soliton-shaped wave packet is unstable in the laboratory environment. It is estimated that a much-larger-scale experimental facility is required to achieve inviscid experiments for the NLS equation.

1. Introduction

Edge waves are one type of trapped-wave phenomenon which occurs near the shore by wave refraction owing to the variable water depth. Edge waves propagate parallel to the shoreline with their crests pointing offshore while their amplitude is maximum at the shore and decays asymptotically to zero in the offshore direction. Wavelengths of edge waves are generally much longer than those associated with incoming waves from offshore. Thus the visual observation of edge waves is usually obscured. Perhaps this less obvious existence of edge waves in the field has prevented the regarding of this wave phenomenon as important for a long time. However, there is now considerable evidence which indicates that edge waves play an important role in coastal flooding, surfbeat phenomena, rip currents, and sedimentology such as the formation of crescentic bars and beach cusps.

Stokes (1846) provided the first analytical evidence for the existence of waves that can propagate along a straight coastline on a beach with a uniform slope. The offshore profile of Stokes' edge waves is an exponential decay with an e folding distance $y_e = (k \cos\beta)^{-1}$, where k is the wavenumber and β is the beach slope from the horizontal. More than one hundred years later, Ursell (1952) showed that there are edge-wave modes other than Stokes' solution. The number of modes depends upon the beach slope with the largest mode number n (a non-negative integer) satisfying

$(2n+1)\beta \leqslant \frac{1}{2}\pi$; the Stokes mode corresponds to $n = 0$. The higher-mode solution also decays asymptotically to zero in the offshore direction but having a node(s) in the offshore profile. The dispersion relation between wave frequency ω and k is given by

$$\omega^2 = gk \sin(2n+1)\beta. \tag{1.1}$$

Using Fourier series expansion for the full water-wave theory, Whitham (1976) proved the existence of weakly nonlinear edge waves of the Stokes mode (they have small but finite wave amplitudes) that continue to propagate parallel to the shore. The dispersion relation for the Stokes mode with the leading order of nonlinear correction is given by

$$\omega^2 = gk \sin\beta\,(1+\tfrac{1}{2}a^2k^2), \tag{1.2}$$

where a is the amplitude of the wave runup on the beach. The form of the dispersion relation (1.2) indicates that weakly nonlinear edge waves are unstable to small perturbation based on an instability criterion given by Whitham (1974, p. 490). Resemblance of (1.2) to the dispersion relation for deep-water waves led Whitham (1976) to infer the existence of edge-wave solitons. His inference can be confirmed by the evolution equation for an envelope of edge waves. Applying the method used by Martin, Yuen & Saffman (1980), the evolution equation for edge waves can be found as follows. Suppose small perturbations of wavenumber k and frequency ω are imposed in (1.2) such that

$$k = k_0 + k', \quad \omega = \omega_0 + \omega', \tag{1.3}$$

where the prime denotes the perturbation, and $\omega_0^2 = gk_0 \sin\beta$. Substitution of (1.3) into (1.2) and keeping terms to second order in the perturbation yields

$$\omega' - \frac{\omega_0}{2k_0}k' + \frac{\omega_0}{8k_0^2}k'^2 - \tfrac{1}{4}\omega_0 k_0^2 a^2 = 0. \tag{1.4}$$

There exists a direct correspondence between the dispersion relation and the governing equation:

$$\partial_t \leftrightarrow -\mathrm{i}\omega', \quad \partial_x \leftrightarrow \mathrm{i}k', \tag{1.5}$$

where x points the propagation (longshore) direction, t is time, and ∂ denotes the partial differentiation with respect to the letter subscript. Then (1.4) can be expressed as operator form:

$$N = \mathrm{i}\left[\partial_t + \frac{\omega_0}{2k_0}\partial_x\right] - \frac{\omega_0}{8k_0^2}\partial_{xx} - \tfrac{1}{4}\omega_0 k_0^2 a^2. \tag{1.6}$$

If this operator N is applied to the complex wave-amplitude parameter A, the evolution equation for progressive edge waves appears to be

$$\mathrm{i}\left[A_t + \frac{\omega_0}{2k_0}A_x\right] - \frac{\omega_0}{8k_0^2}A_{xx} - \tfrac{1}{4}\omega_0 k_0^2 |A|^2 A = 0, \tag{1.7}$$

since $a = |A|$. Equation (1.7) is the nonlinear Schrödinger equation (the NLS equation). Different versions of the derivation of (1.7) were made independently by Akylas (1983) and Yeh (1983).

It is noted that the evolution equation (1.7) for an envelope of the edge waves is identical with that for two-dimensional deep-water waves except that the coefficient of the nonlinear term is one half of that for the deep-water waves. In addition, the evolution process appears to be limited to the longshore direction, i.e. offshore behaviour is not affected. Thus, the behaviour of the evolution process for edge waves

is readily deduced from many studies of the NLS equation for deep-water waves made during the past decade, e.g. by Zakharov & Shabat (1971), Hashimoto & Ono (1972), Lake *et al.* (1977), Ablowitz & Segur (1979), First, a uniform train of edge waves is unstable to a modulational perturbation. This type of instability is well known as the Benjamin–Feir instability for deep-water waves, after Benjamin & Feir (1967). It is also known as the sideband instability because the modulational perturbation manifests itself in the frequency domain as a pair of sidebands around the carrier-wave component. It can be found that a uniform train of edge waves is unstable if the sideband components lie in the range:

$$0 < \delta = \frac{\Delta\omega}{\omega_c} < ak \ll 1, \tag{1.8}$$

where δ measures the frequency separation $\Delta\omega$ of the sideband components from the carrier-wave frequency ω_c. The instability growth in terms of an e folding distance σ_e of propagation is

$$\sigma_e = \{\delta(a^2k^2 - \delta^2)^{\frac{1}{2}} k\}^{-1}. \tag{1.9}$$

The instability with a maximum growth rate occurs at

$$\delta = \tfrac{1}{\sqrt{2}} ak, \tag{1.10}$$

and the e folding distance associated with the maximum growth rate is

$$(\sigma_e)_{\max} = \frac{2}{a^2k^3}. \tag{1.11}$$

It should be noted that the instability range on δ is narrower and the growth rate is slower for the edge waves than for corresponding deep-water waves.

The numerical computations of the nonlinear Schrödinger equation for deep-water waves made by Lake *et al.* (1977) suggests that after the unstable wavetrain reaches a state of maximum modulation, the solution demodulates and eventually returns to the initial unmodulated state. The behaviour of a series of modulation–demodulation cycles associated with the instability of a nonlinear system is known as the Fermi–Pasta–Ulam (FPU) recurrence. Since the edge-wave evolution equation is basically the same as that of the deep-water waves, the FPU recurrence phenomenon is anticipated for the long-time evolution.

Using the inverse scattering transform, Zakharov & Shabat (1971) solved the NLS equation exactly for initial conditions that decay sufficiently fast as $|x| \to \infty$. Zakharov & Shabat showed that any initial packet of deep-water waves eventually evolves into a finite number of envelope solitons and a dispersive train of oscillatory waves. Hence, the existence of edge-wave envelope solitons can be expected with the form:

$$A = a \operatorname{sech}\{ak^2(x - C_g t)\} \exp(\tfrac{1}{8} i\omega_0 a^2 k^2 t). \tag{1.12}$$

Note that the envelope soliton propagates with the linear group velocity C_g of the dominant carrier wave: the amplitude of the envelope soliton and its propagation velocity are independent parameters.

In the present paper, basic properties of progressive edge waves as well as the behaviour predicted by the NLS equation are investigated experimentally in the controlled laboratory environment. Justification and/or shortcomings of the inviscid theory are identified for the boundary-dominated flow phenomenon.

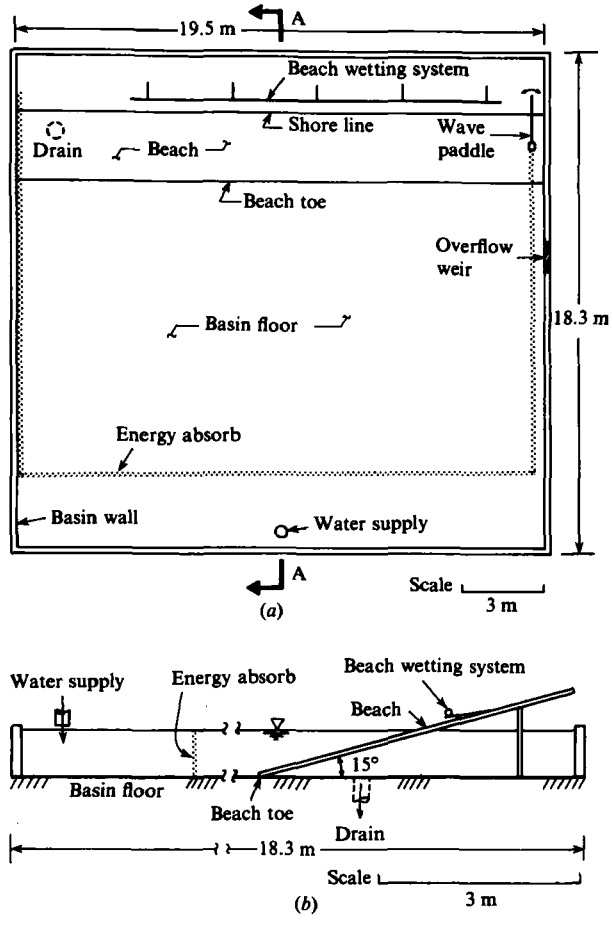

FIGURE 1. Schematic drawings of the basin, beach, and related facilities; (*a*) plan view, (*b*) section A–A view.

2. Experiments

A series of experiments for progressive edge waves of the Stokes mode was conducted in a wave basin 19.5 m wide, 18.3 m long, and 0.76 m deep. Schematic drawings of plan and elevation views of the basin and beach are shown in figure 1. A beach was installed spanning the basin width and is constructed from galvanized sheet steel. In the present study, the slope of the beach was set 15° from the horizontal, $\beta = 15°$. The overflow weir was utilized to skim the water surface continually by providing a slow flow of water into the basin prior to the experiments. The beach-surface wetting system shown in figure 1 is basically a single line sprinkler system that provides an evenly wet condition in the wave runup region on the beach and, more importantly, eliminates possible formation of a water–air–steel contact line at the locus of the maximum runup so that the influence of surface tension there can hopefully be minimized. In fact, it was observed that the waves generated with the treatment of the wetting system have a less distorted sinusoidal profile than those without the treatment. Because of a relatively long wavelength associated with edge waves, it is important to provide a physically large energy-absorption system at the

downstream end of the beach to minimize wave reflection there. The energy-absorption system (not shown in figure 1) consists of seven honeycomb-shaped porous aluminium blocks which are arranged to form the 3.0 m long and 2.4 m wide system. The reflection coefficient of the absorption system is approximately 9% for waves generated in this study, which is sufficient to allow experiments on progressive edge waves. In addition to this energy-absorption system on the beach, sheets of rubberized horse hair are attached to the basin walls to minimize reflections of waves escaped offshore.

The wavemaker is a wedge-shaped paddle that is hinged offshore and oscillates in the longshore direction about the vertical axis. The wave paddle is activated by a hydraulic cylinder, and the hydraulic power unit which drives the cylinder is controlled by the electric servo system. Basically, the overall wave-generating system converts a pre-programmed input electrical signal into the mechanical displacement of the wave paddle. The entire wave-generating system except the wave paddle is installed directly on the laboratory floor outside the basin; thus the mechanical vibrations associated with the system do not disturb the water in the basin.

Wave amplitudes were measured using resistance-type wave gauges. In order to calibrate and position the wave gauge without disturbing the water in the basin, each gauge is mounted on a remote-controlled gauge-positioning system. The gauge position can be changed vertically as well as horizontally using the precision of the stepper motors which are controlled by the system outside of the basin. A more detailed discussion of the laboratory apparatus has been presented by Yeh (1983).

In addition to analog recordings by an oscillograph recorder, digitized wave data are taken with a sampling rate of 25 Hz and are analysed in the frequency domain by means of periodograms. The periodograms are computed for a frequency range of 0–2.44 Hz with a resolution bandwidth of 0.0244 Hz. Analysis of the data in the frequency domain enables us to obtain the quantitative information on the evolution process such as sideband magnitudes, sideband growth rates, sideband frequencies, Similar methodology has been applied to analyse the evolution of deep-water waves by both Lake *et al.* (1977) and Melville (1982).

3. Results

3.1. *Uniform train of edge waves*

We first examine the offshore and longshore characteristics of a uniform train of edge waves. Figure 2 shows experimental results for the offshore amplitude profiles for uniform wavetrains with $\omega = 2.79$ rad/s in the range of the nonlinearity parameter, $0.018 \leqslant ak \leqslant 0.10$. These results are based upon measurements at $x = 12$ m ($kx = 37$) from the wave paddle. The agreement of the measured profiles with the theoretical predictions (exponential decays with $y_e = (k \cos\beta)^{-1}$) provides clear evidence that real progressive edge waves are generated. It should be remarked that absolute magnitudes of the measured wave amplitudes at the offshore locations are extremely small. Perhaps for this reason, the best agreement with the theory is observed for the case with the largest wave amplitude, $ak = 0.10$.

The inviscid theory does not predict any attenuation of edge waves as they propagate. However, wave energy in a real-fluid environment is always dissipated owing to the effect of viscosity so that wave amplitudes attenuate during propagation. Thus, it is necessary to modify the inviscid theory to account for the real-fluid effects before comparison with measured data. A simple model of edge-wave attenuation based on the shallow-water approximation was provided by Guza & Davis (1974).

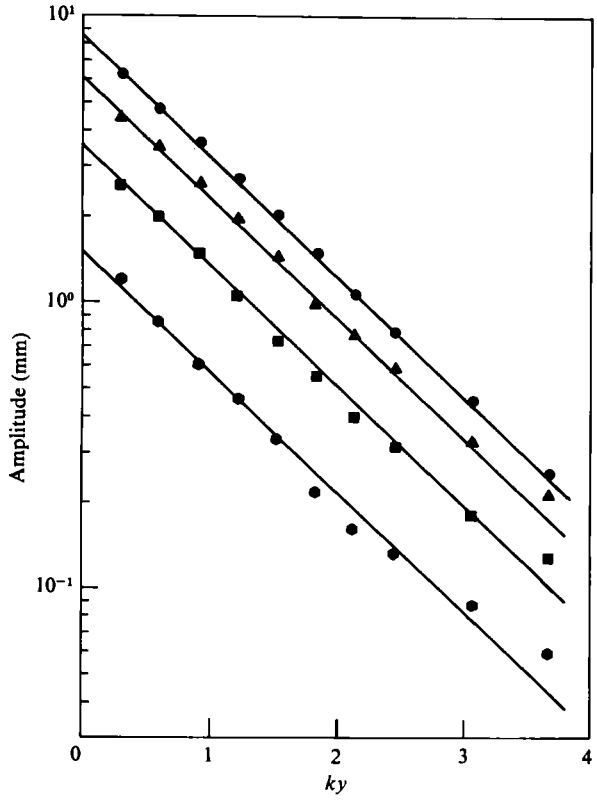

FIGURE 2. Offshore amplitude profiles of edge waves. $\omega = 2.79$ rad/s, $x = 12$ m ($kx = 37$); ●, $ak = 0.10$; ▲, $ak = 0.073$; ■, $ak = 0.043$; ●, $ak = 0.018$; ——, theoretical profile with $y_e = (k \cos\beta)^{-1}$.

They considered the lowest-order viscous effects in thin laminar boundary layers at the (uncontaminated) free surface and the solid bottom boundary of the fluid domain as well as dissipation in the nearly irrotational interior. It was found that dissipation in the bottom boundary layer dominates the edge-wave attenuation, and the edge-wave amplitude is attenuated according to

$$a(kx) = a(0)\,\mathrm{e}^{-2\gamma kx/\omega}, \tag{3.1}$$

where γ is the attenuation rate. Extending the analysis of Guza & Davis to the full water-wave theory, the attenuation rate due to viscous effects at the bottom boundary, γ_b, is found to be

$$\gamma_b = \frac{\nu k^2}{2\sqrt{2}\tan\beta} R^{\frac{1}{2}}, \tag{3.2}$$

in which ν is the kinematic viscosity, and R is the Reynolds number defined by

$$R = \frac{\omega}{\nu k^2}. \tag{3.3}$$

However, considering the present laboratory conditions, the water surface cannot be prevented from contamination. Van Dorn (1966) reported that a 'fully contaminated' surface condition is achieved in a reasonable period of time (hours) when a clean water surface is simply exposed to the atmosphere. In the fully

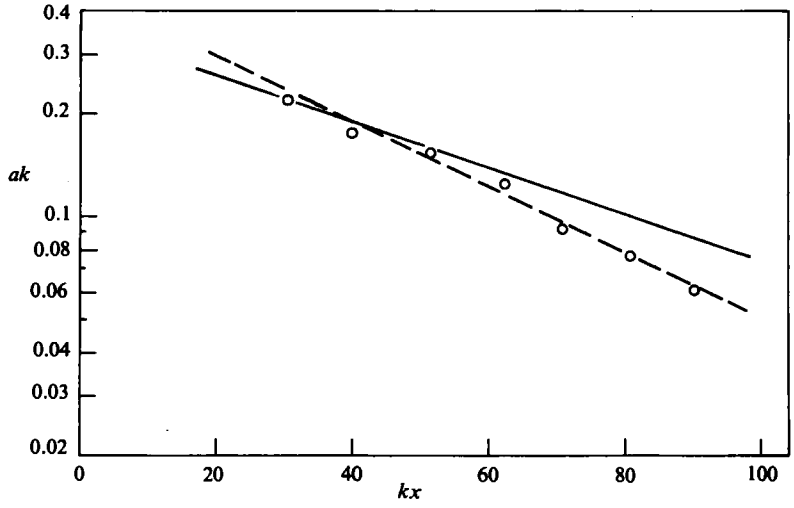

FIGURE 3. Longshore attenuation of wave amplitude. $\omega = 4.05$ rad/s; O, measured data; ——, equation (3.1); – – – –, best fit to the data.

contaminated state, the surface may be regarded as incompressible so that the surface is horizontally immobilized. Thus, its contribution to attenuation is comparable to that of a solid boundary. Considering the fact that the present experiments are reproducible, the water surface must be fully contaminated during the measurements. The attenuation rate due to the fully contaminated surface film can be obtained by a similar manner as used for the bottom boundary layer and is given by

$$\gamma_s = \frac{\nu k^2}{2\sqrt{2}\sin\beta} R_i^{\frac{1}{2}}. \tag{3.4}$$

The combined effects of a contaminated free surface and bottom boundary layer, $\gamma_t = \gamma_s + \gamma_b$, are used in (3.1) to predict the wave attenuation here.

The observed longshore attenuation of amplitude of edge waves with $\omega = 4.05$ rad/s is presented in figure 3. Actual wave amplitudes are measured at $y = 10$ cm ($ky = 0.65$) and are expressed, for the presentation in figure 3, in terms of the parameter ak. Figure 3 shows that the measured rate of attenuation $\gamma_m = 0.0452\ \text{s}^{-1}$ is slightly greater than the theoretical value $\gamma_t = 0.0350\ \text{s}^{-1}$. This discrepancy can be attributed (probably) to dissipation due to the wave runup–rundown process on the beach. For example, formation of an air–water–steel contact line can create water surface curvatures with small radii so that energy transfer to capillary waves may occur there. In fact, capillary waves radiating offshore from the shoreline were observed during experiments. In addition, the flow domain is saturated by the boundary layers near and at the shore, i.e. boundary layers there are not thin. The energy dissipation mechanism at the saturated boundary layer is not known but may contribute to the additional dissipation. (Quantitative estimates of dissipation in the wave runup region are difficult.)

3.2. *Modulational instability*

From an examination of the solutions to the NLS equation (1.7), it was found that a uniform train of progressive edge waves is unstable to a modulational perturbation in their amplitude and frequency, i.e. the modulational feature of an initially uniform

wavetrain is enhanced during propagation. The theoretical predictions for salient features of the instability have already been mentioned and described in (1.8)–(1.11). In order to make quantitative comparisons between the experimental and theoretical results, the effects of viscous dissipation must be considered. (Viscosity is ignored in the theoretical model, while actual wave propagation involves substantial amplitude attenuation as shown in figure 3.) This fundamental discrepancy is often a higher-order effect for experimental studies on water waves. (For example, Lake *et al.* (1977) reported good agreement between theoretical and experimental results on the initial modulational instability of nonlinear deep-water waves. For their carefully controlled experiments, the wave attenuation rate can be estimated based on the assumption that dominant dissipation occurred at the sidewall boundary layers of the tank and in the nearly irrotational interior of the fluid domain. For the wave frequency of 2.5 Hz, the e folding time for the attenuation inferred for the experiments by Lake *et al.* is approximately 360 s. The e folding time for growth of the modulational instability was approximately 6 s in their experiments. Therefore, the effects of wave attenuation were small relative to the inviscid evolution dynamics of a deep-water wavetrain.)

However, a measured value of the attenuation rate for an edge-wavetrain with $\omega = 4.05$ rad/s is $\gamma_m = 0.045\ \mathrm{s}^{-1}$ as presented in §3.1 and corresponding e folding time is 22 s. Using the measured value of $ak = 0.23$ at $x = 5$ m ($kx = 32$) in the experiment presented in figure 3, the e folding time of the theoretical modulational growth is approximately 20 s. Thus, the timescale of the wave attenuation is comparable to that of the inviscid instability. In other words, energy dissipation by viscosity is just as important to the evolution process as the inviscid dynamics on the slow timescale. Thus, the validity of the NLS equation becomes questionable as an appropriate model of the experiments (or *vice versa*). This limitation of the theory (or experiments) is quite important and must be remembered in the theoretical and experimental comparisons which follow.

When the timescale of wave attenuation by viscosity is much longer than that of the inviscid dynamics, the theory can be modified to incorporate the slowly varying effect of attenuation. Although this does not appear to be the case in the present experiments, we will adopt this procedure and then discuss its applicability *a posteriori*. The modification to (1.9) based on linear damping by viscosity yields

$$\sigma_e = \left[\delta\left\{a^2k^2\exp\left(-\frac{4\gamma kx}{\omega}\right) - \delta^2\right\}^{\frac{1}{2}} k\right]^{-1}. \tag{3.5}$$

It should be emphasized that the modified theory above does not take into account nonlinear interactions involving dissipation and should only be regarded as a very rough estimate of the effects.

A uniform train of edge waves is first generated to examine the modulational instability due to background noise in the wave basin. Wave-gauge recordings of amplitude with time at fixed spatial locations are presented in figure 4. The wave amplitudes shown are not equally scaled but their magnitudes can be found from figure 3. These time-domain data show that the initial uniform wavetrain is unstable. At $x = 5$ m ($kx = 32$) the wave record still indicates a uniform wavetrain with no detectable modulation of the amplitude envelope. This uniform wavetrain evolves to a slightly modulated state at $x = 14$ m ($kx = 91$). The modulation parameter δ, defined in (1.8), appears to be approximately 0.1 although it is not clear owing to the small modulation. Even though the instability is detectable in figure 4, the observed growth is fairly small due to (presumably) the limited beach length available for the

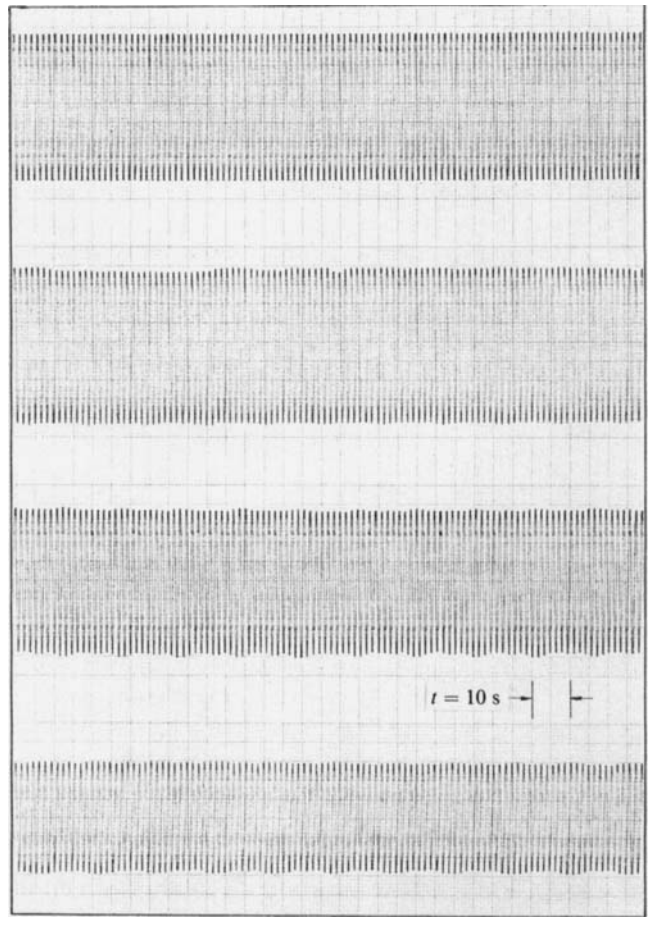

FIGURE 4. Temporal wave profiles at $y = 10$ cm ($ky = 0.65$) for four longshore locations. $\omega = 4.05$ rad/s; (*a*) $x = 5$ m ($kx = 32$), $ak = 0.22$; (*b*) $x = 8$ m ($kx = 52$), $ak = 0.16$; (*c*) $x = 11$ m ($kx = 71$), $ak = 0.09$; (*d*) $x = 14$ m ($kx = 91$), $ak = 0.06$. (Amplitudes shown are not scaled.)

wave propagation. In order to obtain more definitive results, a wavetrain is produced with initial amplitude modulation imposed directly by the programmable wavemaker. Since the instability growth is exponential, the imposed modulation enhances the effects of the instability so as to observe the evolution more clearly along the limited beach length. Almost uniform waves with slight initial modulation of $\delta = 0.167$ are generated and the resulting evolution is presented in figure 5. The value of $\delta = 0.167$ was selected simply because the larger value of δ yields the better resolution on the sidebands for the periodograms (presented later), and $\delta = 0.167$ is still within the unstable range according to (1.8) with the value of nonlinear parameter, $\bar{a}k = 0.19$, at $x = 5$ m ($kx = 32$), where $\bar{a}$ is the time-averaged runup amplitude. Figure 5 indicates that a very slight amplitude modulation observed at $x = 5$ m ($kx = 32$) evolves to the much stronger modulation at $x = 14$ m ($kx = 91$). This behaviour provides clear qualitative evidence for the instability of modulational perturbation as predicted by the theory. The corresponding periodograms are shown in figure 6. The ordinate of a periodogram represents the modulus-squared of the finite Fourier transform of a time series; thus, in the normalized form in figure 6, the parameter S

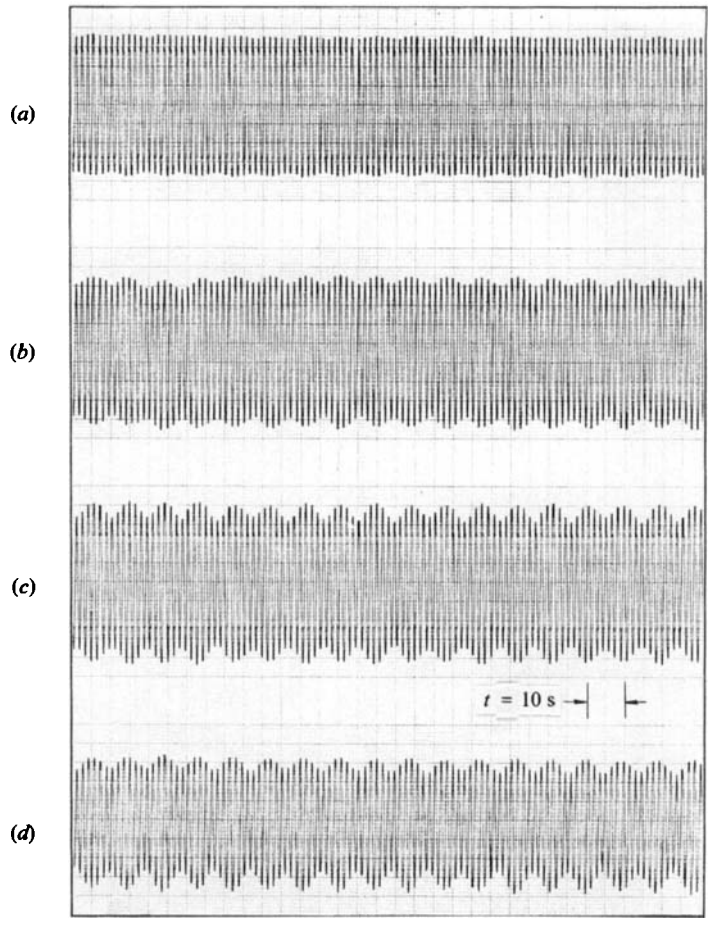

FIGURE 5. Temporal wave profiles at $y = 10$ cm ($ky = 0.65$) for four longshore locations of a wavetrain with an initially imposed amplitude modulation, $\delta = 0.167$, $\omega = 4.05$ rad/s; (*a*) $x = 5$ m ($kx = 32$), $\bar{a}k = 0.19$; (*b*) $x = 8$ m ($kx = 52$), $\bar{a}k = 0.13$; (*c*) $x = 11$ m ($kx = 71$), $\bar{a}k = 0.07$; (*d*) $x = 14$ m ($kx = 91$), $\bar{a}k = 0.05$. (Amplitudes shown are not scaled.)

represents the wave amplitude normalized by that at the carrier wave frequency ω_c. The magnitude of the modulation is quantitatively measured by the parameter S^2 at the sideband frequencies. It is noted that the use of the normalized parameter S^2 removes the first-order effect of dissipation. The sequence of periodograms in figure 6 shows the sideband growth with propagation from the initially (almost) uniform wavetrain, but the growth seems to be limited to the lower sideband component only. Variations of the parameter S^2 with the propagation distance for both upper- and lower-sideband components are presented in figure 7 together with the corresponding theoretical prediction for damped growth given by (3.5). It should be noted that the theoretical curve of the inviscid growth given by (1.9) would be a straight line in the figure but is not presented here since the effective value of ak cannot be identified due to its rapid decay. (However, note that a slope of the damped growth curve represents the inviscid growth rate based on the local value of ak.) Figure 7 shows an exponential growth of the lower sideband component with a constant rate; the e folding distance for the measured growth is $\sigma_e = 7.3$ m. The lower

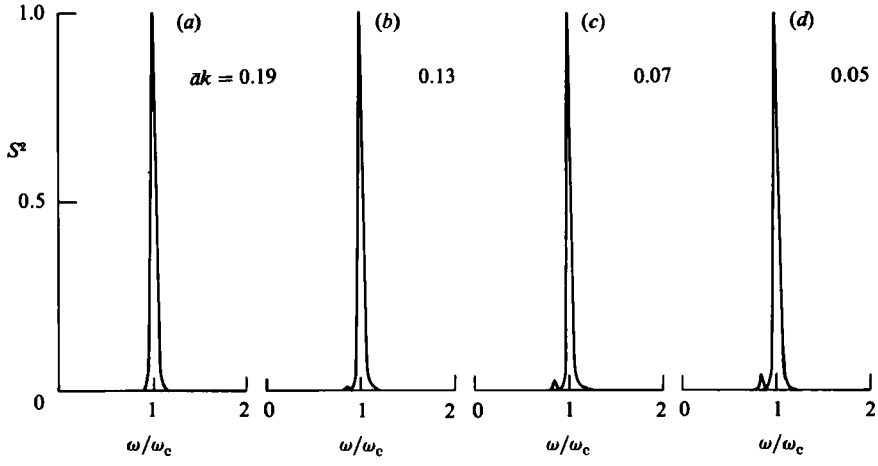

FIGURE 6. Periodograms of wave records shown in figure 5.

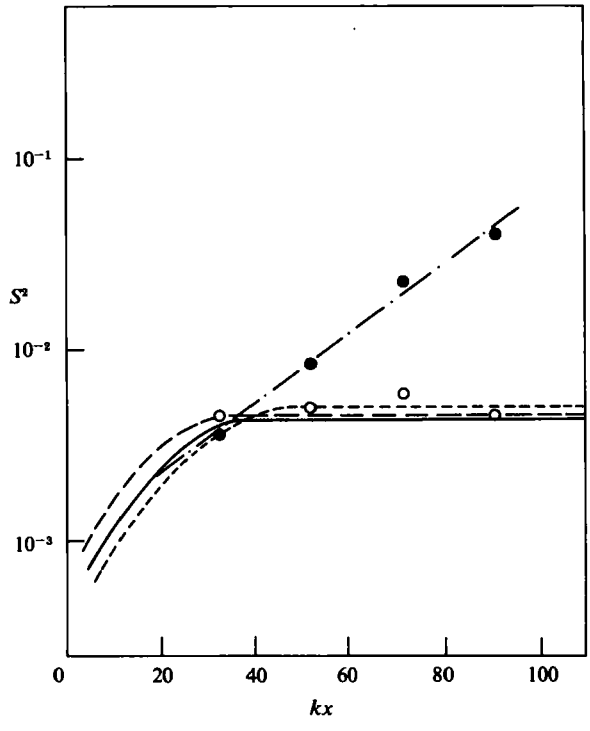

FIGURE 7. Variation of normalized sideband amplitudes with propagation distance. ●, lower sideband; ○, upper sideband; ——, theory (equation (3.5)); –·–, measured growth ($\sigma_e = 7.1$ m); – – –, (3.5) using upper-sideband attenuation; ------, (3.5) using lower-sideband attenuation.

sideband continues to grow even when the local value of wave nonlinearity becomes very small, e.g. $\bar{a}k = 0.05$ at $kx = 91$. No such exponential growth of the upper sideband can be observed; its magnitude S^2 is essentially constant during propagation. The damped growth given by (3.5) eventually predicts no growth, in agreement with the measured upper sideband behaviour but not with the lower sideband behaviour. The inviscid and modified inviscid theories of (1.9) and (3.5) which

predict equal growth of both sideband components totally fail to describe the diverging trend of the measured upper- and lower-sideband components.

A diverging trend of sideband amplitudes during evolution is not unique to the present experimental results on edge waves. Such a phenomenon was also observed for deep-water waves by both Lake *et al.* (1977) and Melville (1982). According to their similar experimental results, both sideband components grow exponentially with the same rate in the early stage of evolution. However, after the wavetrain modulates substantially ($S^2 \approx 0.1$), sideband growth slows down but each sideband decelerates with a different rate; the amplitude of the upper sideband becomes smaller than that of the lower sideband. The deceleration of growth continues until both sidebands fall to local minima at which time they then begin growing again. Melville added that this divergence of the sideband amplitudes occurred in the neighbourhood of the onset of wave breaking observed in his experiments and the local minima corresponded to the cessation of breaking. In this basis, Melville suggested that the diverging behaviour was caused by wave breaking since the breaking instability is selective over the relatively small frequency difference between sidebands. The breaking mechanism cannot be an explanation for the similar behaviour observed for edge waves since no breaking occurred in these experiments. The energy dissipation involved in the edge-wave experiments is large but the effects are smooth in time rather than abrupt as in wave breaking. Perhaps this is why the results presented in figure 7 are orderly compared to the transient behaviour of the sidebands observed during wave breaking for the deep-water wavetrain. According to a linear analysis, viscous effects are not so selective over the relatively small frequency difference between sidebands. In order to demonstrate this, the theoretical damped growth of (3.5) using viscous dissipation for each sideband component is shown in figure 7 (although the use of a dissipation term in (3.5) other than that for a carrier-wave component does not have a clear theoretical basis). However, this linear analysis for the viscous effects might not conform to the present situation where the timescale of dissipative effects is comparable with that of the inviscid instability, so that the nonlinear interactions involving dissipation may be important.

3.3. *Long-time evolution*

As discussed in §1, numerical computations of the nonlinear Schrödinger (NLS) equation by Lake *et al.* (1977) implied the Fermi–Pasta–Ulam recurrence phenomenon for the long-time evolution of edge waves. However, reliability of this prediction for edge waves is questionable in the laboratory environment because of substantial viscous dissipation present in the evolution process. It is even uncertain if consideration of the subject itself is relevant since the evolution process may not reach a 'long-time' stage maintaining its nonlinear characteristics.

In order to observe the long-time evolution of a deep-water wavetrain in the limited length of a wave tank, Lake *et al.* (1977) conducted a series of experiments using wavetrains having fixed values of a carrier-wave frequency ω_c, initial wave nonlinearity parameter $(ak)_0$, and sideband separation parameter δ. The only difference between the individual experiments was that each was performed imposing different magnitudes of sidebands at the wavemaker. These measurements were then patched together to obtain the evolution in an 'effectively' longer wave tank. This procedure is only possible for studying the long-time behaviour of inviscid dynamics when dissipative effects are so small that the fixed value of $(ak)_0$ used in each experiment does not create significant discontinuity in the patched results. The rapid reduction of amplitude by viscosity in the edge-wave experiments prohibits the study of the

evolution in an 'effectively' longer wave tank by patching the results because of the significant discontinuity involved in ak. Despite this drawback, we conducted a series of experiments using successive wavetrains with a fixed value of $(ak)_0$ but varying strengths of the initial modulation, just as performed by Lake *et al.* for deep-water waves. Instead of patching, we initially examined the results of each experiment separately to see the impact of large modulation of a uniform train.

Wave gauge recordings at the distance $y = 10$ cm ($ky = 0.65$) for wavetrains with $\omega_c = 4.05$ rad/s, $\delta = 0.167$, and various strengths of the initial modulation are presented in figure 8. In order to identify each wavetrain generated, the parameter S_p is introduced here, which represents a sideband amplitude normalized by that at a carrier frequency for the imposed wave paddle motion itself. The wavetrains presented in figures 8(*a*), (*b*), and (*c*) are generated with $S_p = 0.10$, 0.29, and 1.0 respectively. (Incidentally, the wavetrain presented in figure 5 is generated with $S_p = 0.025$.) As shown in figures 8(*a*) and (*b*), the amplitude modulations are enhanced during propagation for the wavetrains generated with $S_p = 0.10$ and 0.29. Each wave packet for $S_p = 0.29$ is eventually 'pinched out' from the adjacent packet. On the other hand, the wavetrain generated with $S_p = 1.0$ (full node-to-node modulation) demodulates and appears to be evolving toward an unmodulated state. This behaviour in the time-domain data corresponds qualitatively to that of Fermi–Pasta–Ulam recurrence. In order to clarify the quantitative behaviour of wavetrains, the corresponding periodograms are shown in figure 9. Figure 9(*a*) shows an instability behaviour similar to that observed in figure 6 but with more enhanced sideband amplitudes. Again, growth is limited to the lower-sideband component. Figure 9(*b*) shows growth of the lower-sideband component which eventually outgrows the amplitude of the carrier wave at $kx = 91$. In figure 9(*c*), the amplitude of the lower-sideband component exceeds that of the carrier wave initially at $kx = 32$. Nevertheless, the lower sideband continues to grow and the amplitude becomes approximately 100 times that of the original carrier wave at $kx = 91$. Apparently, the lower sideband assumes the role of the carrier wave as a shift of energy to lower frequency occurs. Figure 9(*c*) also shows the emergence of a new lower-sideband component at a frequency with the same separation $\Delta\omega$. According to the sequence of periodograms in figure 9(*c*), the demodulation process observed in the time domain of figure 8(*c*) is a consequence of continuous growth of the lower-sideband component and is not genuine Fermi–Pasta–Ulam recurrence as predicted by the inviscid theory. The observed demodulation process involves a frequency shift to the lower value. A similar frequency shift of a carrier wave was also observed by Melville (1982) in his experiments for deep-water waves which involved much smaller viscous dissipation than that for edge waves. He attributed the frequency shift to wave breaking. Again, the breaking mechanism cannot be an explanation here since no breaking occurred in the present experiments; however, substantial energy dissipation is caused by direct viscous effects. Although direct viscous dissipation is small for deep-water waves, turbulence induced by wave breaking must cause a large energy dissipation. Thus, a common factor of edge-wave and deep-water-wave evolutions is the involvement of substantial energy dissipation even though the dissipation mechanisms are different. Therefore, we conjecture that the frequency down-shift phenomenon for edge waves is a consequence of nonlinear viscous dissipation effects although the nature of the dissipation process is still unclear. (The evolution equation including the strong viscous effects is not known.)

It is noted also that the results of the three separate experiments shown in figures 8 and 9 seem to be those taken from a single experiment over a long propagation

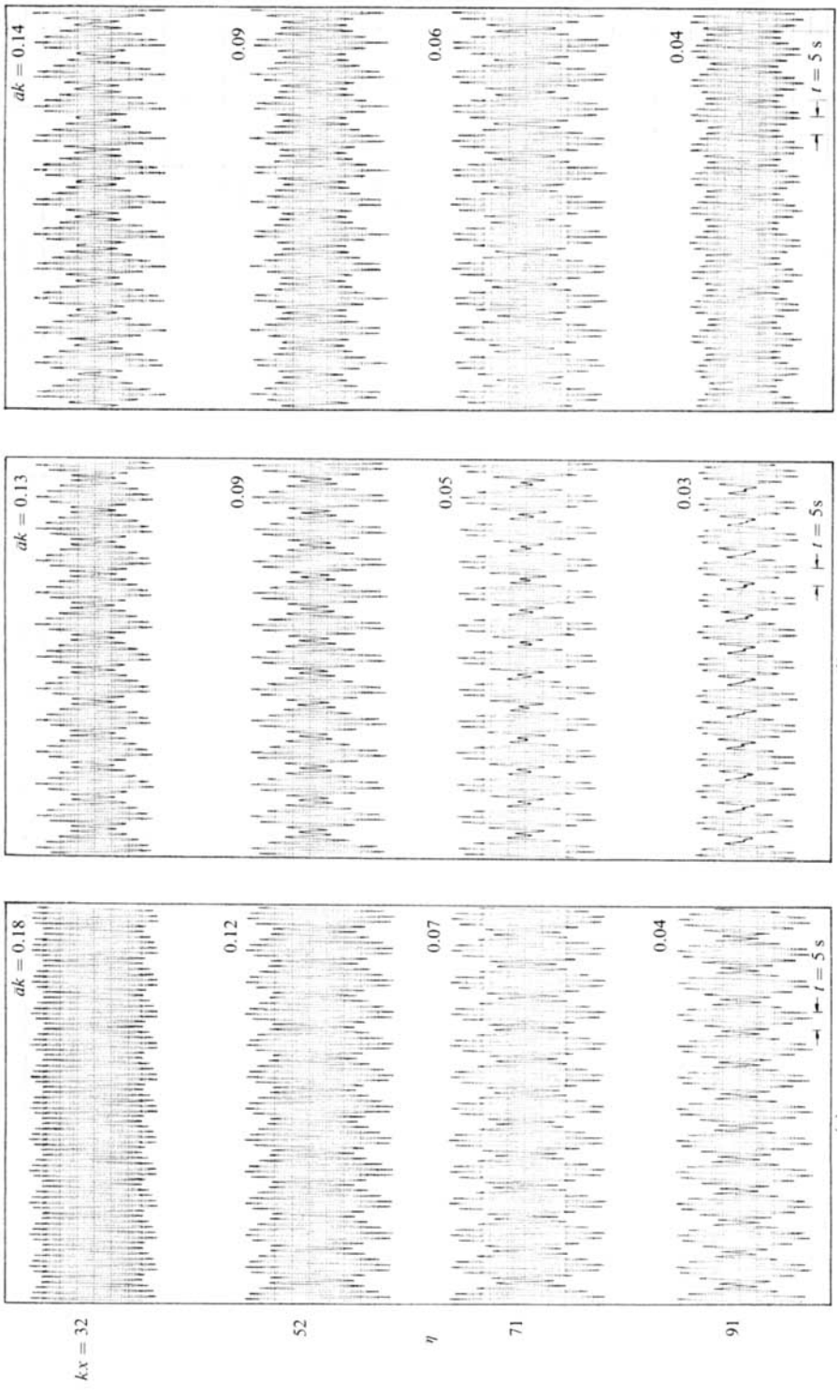

FIGURE 8. Temporal wave profiles at $y = 10$ cm ($ky = 0.65$) for four locations of a wavetrain with $\omega_c = 4.05$ rad/s, $\delta = 0.167$; (*a*) $S_p = 0.10$; (*b*) $S_p = 0.29$; (*c*) $S_p = 1.0$. (Amplitudes shown are not scaled.)

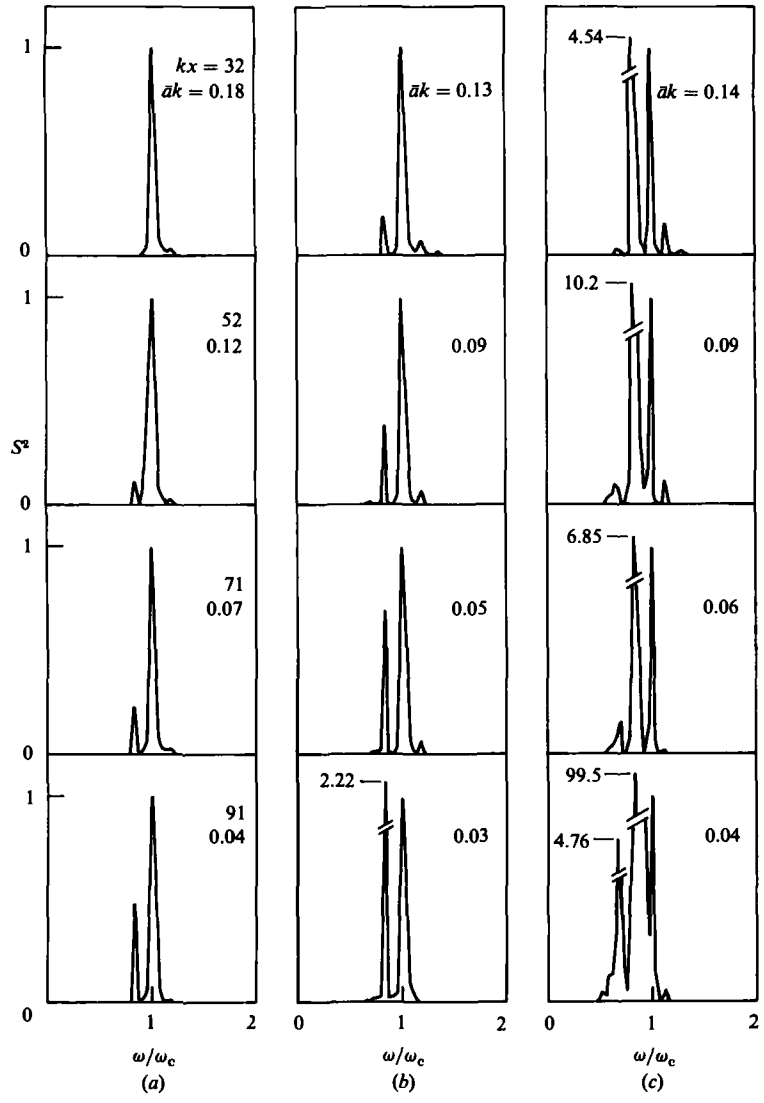

FIGURE 9. Periodograms of wave records shown in figure 8.

distance when viewed from one perspective. For example, the periodogram at $kx = 32$ in figure 9 (*b*) resembles that at $kx = 71$ in figure 9 (*a*), and the periodograms at $kx = 91$ in figure 9 (*b*) and at $kx = 32$ in figure 9 (*c*) are similar (although corresponding values of $\bar{a}k$ are substantially different). Variations of the normalized magnitudes S^2 of the lower-sideband component for these three experiments are presented in figure 10 (*a*). Included here also are the results presented in figure 7. The growth pattern of each experiment shown is smooth and qualitatively consistent with each other. Thus, we attempted to patch the results together to produce a composite evolution process for the lower-sideband component. Such an attempt is made by shifting the results until a single smooth pattern appears. The results are presented in figure 10 (*b*). The solid line in this figure is the measured exponential growth rate of the lower sideband with the *e* folding distance $\sigma_e = 7.3$ m. The consequence of this shifting is surprising. The lower-sideband component grows exponentially with a constant rate regardless of

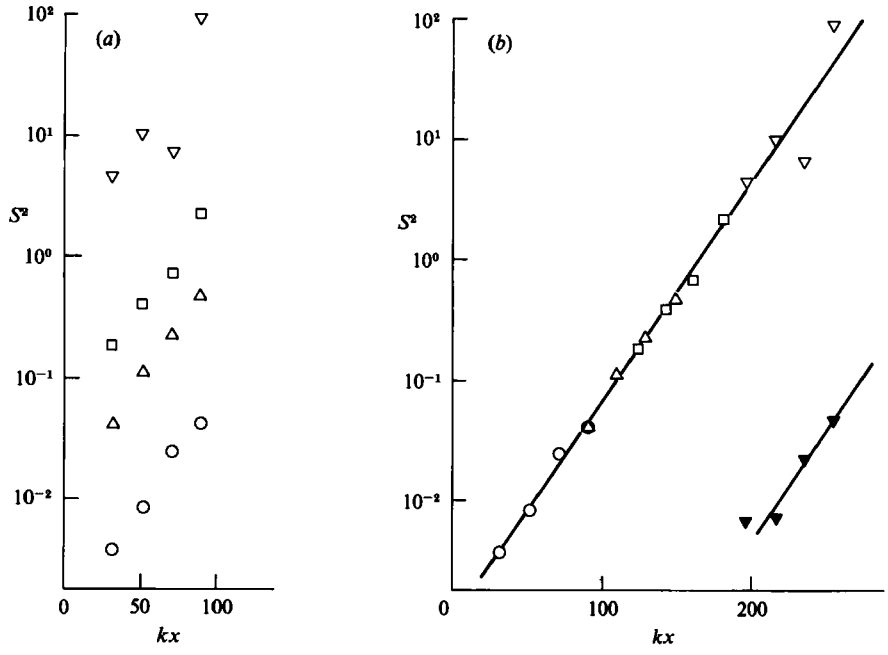

FIGURE 10. Variation of normalized lower-sideband amplitudes, (*a*) with propagation distance and (*b*) in a patched form found by shifting data in space, $\omega_c = 4.05$ rad/s, $\delta = 0.167$; ○, $S_p = 0.025$; △, $S_p = 0.10$; □, $S_p = 0.29$; ▽, $S_p = 1.0$; ▼, $S_p = 1.0$ for newly emerged lower sideband; ——, measured growth with $\sigma_e = 7.1$ m.

initial modulation. This is true even after the lower sideband outgrows the carrier-wave component. For $S^2 > 1.0$, the original lower-sideband component becomes effectively a carrier-wave component and as a result a frequency shift occurs. Then the results for $S^2 > 1.0$ are viewed as showing that the original carrier-wave component (or shifted upper-sideband component) decays exponentially with the same rate from the fully modulated state. Values of S^2 for the newly born lower-sideband component shown in figure 9 (*c*) are also presented in figure 10 (*b*). Again, the growth pattern seems to follow that of its predecessor. It should be re-emphasized here that the wave nonlinearity is not continuous between the patched experimental results presented.

Unlike the behaviour of the lower sideband, no exponential growth is observed for the upper-sideband component. Shifting the data spatially to produce a composite evolution pattern is not possible for the upper-sideband behaviour.

3.4. *Edge-wave envelope solitons*

The NLS equation of (1.7) predicts the existence of edge-wave envelope solitons. Soliton phenomena in the context of water waves have been studied experimentally by Hammack & Segur (1974) and Weidman & Maxworthy (1978) for long waves, Koop & Butler (1981) and Segur & Hammack (1982) for long internal waves, as well as Yuen & Lake (1975) and Ablowitz & Segur (1979) for deep-water waves. In all of these experiments the effects of viscosity were weak relative to the inviscid dynamics of wave dispersion and nonlinearity. Consequently, the solitons evolved in the viscous environments and then slowly decayed in amplitude. During decay the soliton continually adjusted its shape to retain the proper amplitude–length relationship to remain 'locally' a soliton. It is noted that the timescale for long-wave

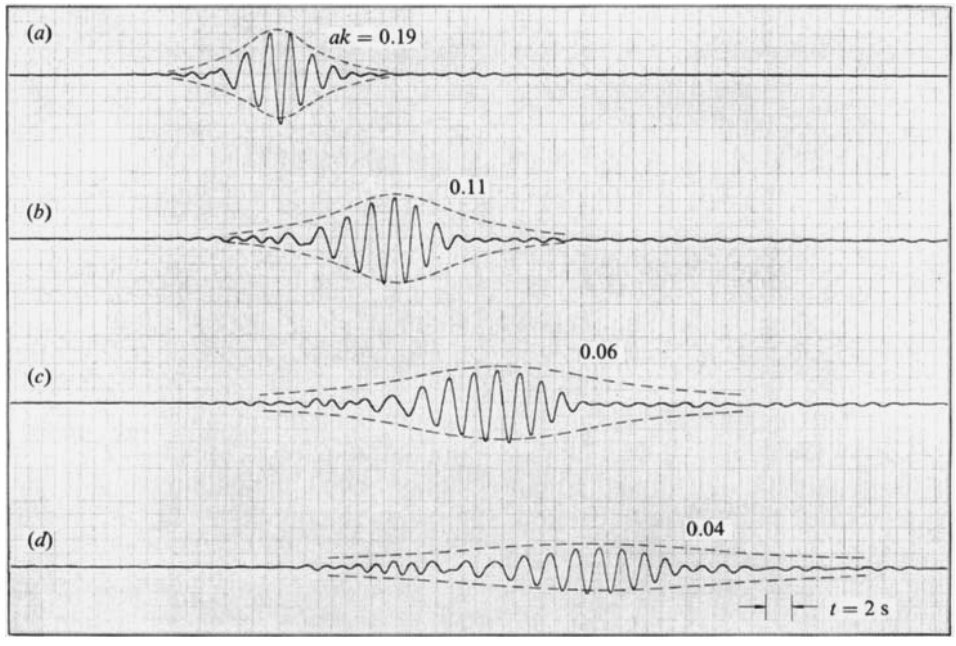

FIGURE 11. Temporal wave profiles at $y = 10$ cm ($ky = 0.65$) for four longshore locations with an initial soliton-shaped packet, $\omega_c = 4.05$ rad/s; (*a*) $x = 5$ m ($kx = 32$); (*b*) $x = 8$ m ($kx = 52$); (*c*) $x = 11$ m ($kx = 71$); (*d*) $x = 14$ m ($kx = 91$); ------, theoretical envelope profile (Eq. (1.12)). (Amplitudes shown are not scaled.)

solitons to occur, $O(ak)$, is much shorter than that, $O(a^2k^2)$, for deep-water or edge-wave solitons governed by the nonlinear Schrödinger (NLS) equation. Thus, the timescale of viscous attenuation for long-wave solitons can be much shorter than that for the envelope solitons of the NLS equation without significantly affecting the inviscid dynamics. Segur (1981) also showed that envelope solitons of deep-water waves decay twice as fast by viscous effects as the corresponding uniform train of infinitesimal waves. This causes additional difficulty in achieving a timescale separation between viscous and inviscid dynamics for solutions governed by the NLS equation.

As noted in §3.2, viscous effects on uniform trains of edge-waves are not weak relative to the inviscid effects modelled by the NLS equation. Since viscous effects are expected to be even greater for envelope solitons, it is legitimate to question the existence of even 'locally' edge-wave envelope solitons. Using the carrier wave frequency $\omega = 4.05$ rad/s edge-waves with an envelope given by (1.12) are generated. Because of the wave attenuation involved and the lack of a solution to the wavemaker problem, the effective magnitude of the wave nonlinearity parameter ak and the corresponding lengthscale of the envelope soliton must be determined by trial and error. The wavemaker stroke and envelope length- (time-) scale are varied until the envelope profile at the first measurement station at $x = 5$ m ($kx = 32$) conforms to (1.12), i.e. a local soliton structure is achieved, as seen in figure 11. During the subsequent propagation the initially soliton-shaped envelope distorts and appears as a wave packet(s) of asymmetric shape. These results are typical of all efforts to generate a 'locally' envelope soliton. Thus, it does not appear that a locally-soliton wave packet is stable in the laboratory environment used here. Viscous attenuation apparently influences the inviscid dynamics to prevent wave nonlinearity from

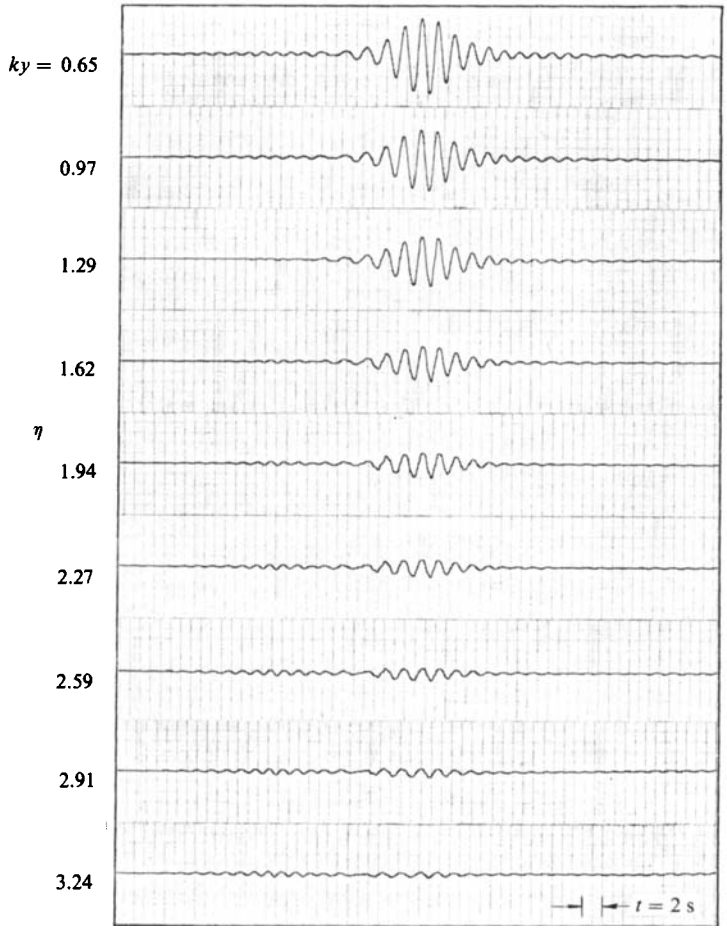

FIGURE 12. Temporal wave profiles at $x = 11$ m ($kx = 71$) at various offshore locations for a symmetrical wave packet with $\omega_c = 4.05$ rad/s. (Amplitudes shown are not scaled.)

balancing with linear effects of frequency dispersion. The measured exponential attenuation rate for the envelope shown in figure 11 is $\gamma_m = 0.059$ s^{-1} which exceeds the measured attenuation rate for the corresponding uniform train presented in figure 3 by approximately 30 %.

It should be noted that Akylas (1983) showed that an envelope soliton for edge waves has a three-dimensional structure and is dependent of the vertical and offshore coordinates; the decay rate in the offshore direction is diminished due to the nonlinear effects and the phase of an envelope soliton depends on the offshore and vertical coordinates. However, his solution (equation (54) in Akylas 1983) contains a singularity as $ak^2(y\cos\beta - z\sin\beta) \to \frac{1}{2}\pi$ so that it is not clear that his solution is correct. Although Akylas' theoretical prediction cannot be compared with the present experimental results (since no envelope soliton could be generated), it is interesting to examine the offshore behaviour of a single symmetrical wave packet at a downstream beach location. The profiles at 9 offshore locations of this symmetrical wave packet at $x = 11$ m ($kx = 71$) are shown in figure 12. The results indicate that the symmetrical envelope shape is consistent at the offshore locations. The amplitude

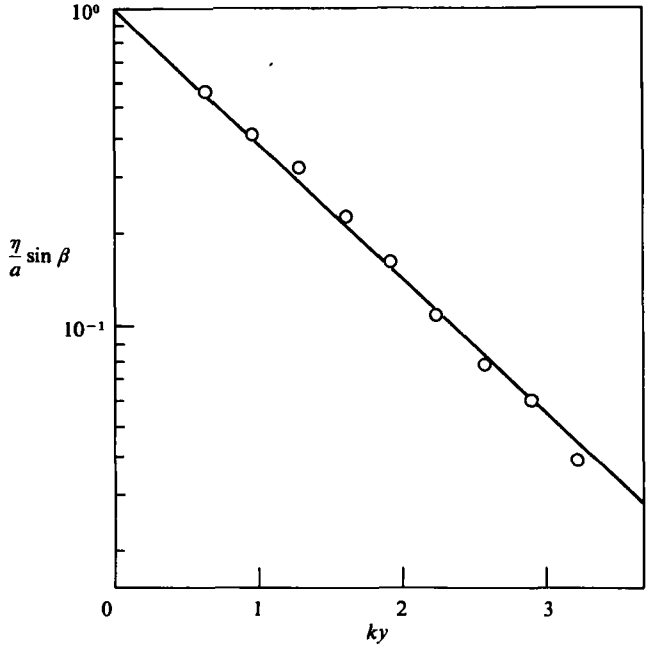

FIGURE 13. Offshore amplitude profile of the symmetric wave packet shown in figure 12. ○, measured data; ——, theoretical profile.

of the envelope decays exponentially offshore with the theoretical e folding distance, $y_e = (k\cos\beta)^{-1}$, as shown in figure 13. Based on these data, there appears to be no three-dimensional structure for the envelope and no unstable behaviour in the offshore (transverse) direction.

Careful observation of the results in figures 11 and 12 reveals that there exists a small wave packet leading the main wave group. Unfortunately, the offshore profile of this wave packet cannot be measured due to its small amplitude, although inspection of figure 12 indicates the appearance of a node. The phase velocity C_p for this packet was measured by aligning the two wave gauges parallel to the shoreline with a spacing of 50 cm apart; the result was found to be $C_p = 1.8$ m/s. This measured phase speed closely agrees with the theoretical value $C_p = 1.7$ m/s for the higher-mode ($n = 1$) edge waves. The appearance of a node in the offshore profile and the phase speed suggest that the small wave packet consists of edge waves of the higher mode. The higher-mode edge waves must be generated by the wavemaker motion, and the faster propagation and less wave attenuation associated with the higher mode enhance its appearance at the downstream location.

4. Conclusion

We first showed that progressive edge waves can in fact be generated directly in a laboratory wave tank. The amplitude of progressive edge waves attenuates exponentially as they propagate. The actual attenuation rate is greater than the theoretical prediction based on the lowest-order dissipation mechanism of laminar boundary layers at the beach surface and the free water surface (fully contaminated). The timescale of the wave attenuation in the experiments is comparable with the timescale of the evolution process for weakly nonlinear and inviscid progressive edge

waves modelled by the NLS equation. This fact emphasizes the shortcomings of the derived evolution equation as an appropriate model of the experiments (or vice versa). Although the NLS equation indicates the occurrence of instability for a uniform train of edge waves, the actual behaviour of the unstable wavetrain is qualitatively and quantitatively different from the theoretical predictions. For the unstable wavetrain, the theory predicts that a pair of sideband components around the carrier-wave frequency should grow exponentially at an equal rate. The actual behaviour of the sideband components is as follows. The lower-sideband component grows exponentially at a constant rate. The upper-sideband component experiences no growth. This behaviour of each sideband is not limited to the initial instability of a uniform wavetrain, but is also the same for an initially modulated wavetrain. Furthermore, the exponential growth rate of the lower sideband appears to be independent of the strength of the initial modulation. Depending on the initial modulation, the lower-sideband component can even outgrow the carrier-wave component and, as a result, the initially modulated wavetrain demodulates with shifting of the frequency of the dominant wave to a lower value. Similar behaviour of the frequency downshift has also been observed for deep-water waves with weak viscous effects but involving wave breaking. No wave breaking occurred in the edge-wave experiments but viscous effects are substantial for edge waves. Since both wave breaking for deep-water waves and direct viscous effects for edge waves cause significant energy dissipation, we conjecture that this frequency down-shift phenomenon is a consequence of nonlinear dissipation effects which are not modelled by the inviscid theory (the NLS equation).

The NLS equation also indicates the existence of edge-wave envelope solitons. However, a generated soliton-shaped wave packet distorts and becomes asymmetric during propagation. In other words, locally soliton-shaped packets of edge waves are unstable in the laboratory environment. Viscous attenuation appears to decrease wave nonlinearity too rapidly for it to remain balanced locally with the linear effect of frequency dispersion. On the other hand, a symmetrical wave packet observed near the shore is consistent at the offshore locations. The amplitude of the envelope decays exponentially offshore in accordance with the linear theory.

In order to achieve inviscid experiments for the NLS equation, the timescale of the viscous effects must be much smaller than the timescale of the evolution process, i.e.

$$\gamma_t \ll \tfrac{1}{4}\omega a^2 k^2. \tag{4.1}$$

Taking the smallness to be $O(ak) \ll 1$, (4.1) can be expressed by

$$\omega < O\left(\frac{a^2 k^2 g^{\frac{1}{3}} \beta^{\frac{4}{3}}}{2\nu^{\frac{1}{3}}}\right) \tag{4.2}$$

as a criterion for the inviscid experiments with small β. The wave frequency should be less than 1.5 rad/s for the viscous effects to be unimportant under the conditions of $\beta = 15°$ and $ak = 0.2$. The corresponding e folding distance for the maximum instability growth rate of a uniform edge-wavetrain is 56 m. This would require an extremely large wave tank, say 150 m long; the propagation distance should be at least several times the e folding distance in order to observe the evolution process. Such experiments are not possible in the laboratory facility used in this study. On the other hand, edge-wave frequencies are relatively small for field conditions (e.g. $\omega \approx 0.05$ rad/s observed by Huntley, Guza & Thornton 1981). Hence the viscous distortion on the evolution process should not be a problem unless the beach slope is extremely small, and the present experimental results cannot disprove the application of the inviscid theory to the field conditions. As demonstrated by these

estimates, the scale effects are important in laboratory experiments for this boundary-dominated flow. It is interesting to note that significant scale effects were also pointed out by Sprinks & Smith (1983) who analysed the experimental results for wave amplification at a conical island, which is another type of boundary-dominated flows.

The author is indebted to Professor J. L. Hammack for suggesting this topic and for helpful discussions. The work for this paper was supported in part by the University of California, Berkeley, and by National Science Foundation Grant no. ENG-781/697.

REFERENCES

Ablowitz, M. J. & Segur, H. 1979 On the evolution of packets of water waves. *J. Fluid Mech.* **92**, 691–715.

Akylas, T. R. 1983 Large-scale modulation of edge waves. *J. Fluid Mech.* **132**, 197–208.

Benjamin, T. B. & Feir, J. E. 1967 The disintegration of wave trains on deep water. Part 1. Theory. *J. Fluid Mech.* **27**, 417–430.

Guza, R. T. & Davis, R. E. 1974 Excitation of edge waves by waves incident on a beach. *J. Geophys. Res.* **79**, 1285–1291.

Hammack, J. L. & Segur, H. 1974 The Kortweg–de Vries equation and water waves. Part 2. Comparison with experiments. *J. Fluid Mech.* **65**, 289–314.

Hashimoto, H. & Ono, H. 1972 Nonlinear modulation of gravity waves. *J. Phys. Soc. Japan* **33**, 805–811.

Huntley, D. L., Guza, R. T. & Thornton, E. B. 1981 Field observations of surf beat 1. Progressive edge waves. *J. Geophys. Res.* **86**, 6451–6466.

Koop, C. G. & Butler, G. 1981 An investigation of internal solitary waves in a two-fluid system. *J. Fluid Mech.* **112**, 225–251.

Lake, B. M., Yuen, H. C., Rungaldier, H. and Ferguson, W. E. 1977 Nonlinear deep-water waves: theory and experiment. Part 2. Evolution of a continuous wave train. *J. Fluid Mech.* **83**, 49–74.

Martin, D. U., Yuen, H. C. & Saffman, P. G. 1980 Stability of plane wave solutions of the two-space-dimensional nonlinear Schrödinger equation. *Wave Motion* **2**, 215–229.

Melville, W. K. 1982 The instability and breaking of deep-water waves. *J. Fluid Mech.* **115**, 165–185.

Segur, H. 1981 Viscous decay of envelope solitons in water waves. *Phys. Fluids* **24**, 2372–2374.

Segur, H. & Hammack, J. L. 1982 Soliton models of long internal waves. *J. Fluid Mech.* **118**, 285–304.

Sprinks, T. & Smith, R. 1983 Scale effects in a wave-refraction experiment. *J. Fluid Mech.* **129**, 455–471.

Stokes, G. G. 1846 Report on recent researches in hydrodynamics. *Rep. 16th meeting Brit. Assoc. Adv. Sci.*, pp. 1–20. In *Math. & Phys. Papers*, **1**, 157–187, Cambridge, 1880.

Ursell, F. 1952 Edge waves on a sloping beach. *Proc. R. Soc. Lond.* A **214**, 79–97.

Van Dorn, W. G. 1966 Boundary dissipation of oscillatory waves. *J. Fluid Mech.* **24**, 769–779.

Weidman, P. D. & Maxworthy, T. 1978 Experiments on strong interactions between solitary waves. *J. Fluid Mech.* **85**, 417–431.

Whitham, G. B. 1974 *Linear and Nonlinear Waves*. New York: Wiley-Interscience.

Whitham, G. B. 1976 Nonlinear effects in edge-waves. *J. Fluid Mech.* **74**, 353–368.

Yeh, H. 1983 Nonlinear edge-waves. *Rep. No.* UCB/HEL-83/04, University of California, Berkeley.

Yuen, H. C. & Lake, B. M. 1975 Nonlinear deep water waves: Theory and experiment. *Phys. Fluids* **18**, 956–960.

Zakharov, V. E. & Shabat, A. B. 1971 Exact theory of two-dimensional self-focusing and one-dimensional self-modulation of waves in nonlinear media. *Zh. Eksp. Teor. Fiz.* **61**, 118–134. Translated in *Sov. Phys., J. Exp. Theor. Phys.* **34**, 62–69 (1972).